

Effect of Large-Angle Scattering between Ions and Neutral Particles on the Density Profile at the Divertor Plate^{*)}

Daisuke UMEZAKI and Hideaki MATSUURA

*Department of Applied Quantum Physics and Nuclear Engineering,
Kyushu University, 744 Motooka, Fukuoka 819-0395, Japan*

(Received 16 November 2020 / Accepted 14 January 2021)

The better radial transport modelling of the SOL/divertor plasmas is required to obtain quantitative agreements between experimental values and simulation results towards the proper SOL/divertor plasma prediction of the future magnetic fusion devices. Various SOL/divertor codes (e.g. SONIC, SOLPS-ITER, EDGE2D, UEDGE, EMC3-Eirene, etc.) have been developed and applied to the interpretative simulations of the present fusion devices. Above codes treats the radial transport as a diffusion model and there exists uncertainty to decide the value of the diffusion coefficients. The simulation by the SONIC has resulted in a few times larger ion flux towards the divertor plate than the experimental value observed in JT-60U possibly due to such an uncertainty of the diffusion process. To achieve the quantitative agreement between the experiments and the simulation results is indispensable to predict SOL/divertor plasma parameters of the future fusion devices. Here, radial transport was simulated by considering large-angle elastic scattering between ions and neutral particles and by applying the probability distribution function to fluid equations in the divertor plasma. It was found that the density peak and ion flux are reduced by about half.

© 2021 The Japan Society of Plasma Science and Nuclear Fusion Research

Keywords: divertor, edge plasma, SOL, large-angle scattering, elastic scattering

DOI: 10.1585/pfr.16.2403021

1. Introduction

Various SOL/divertor codes have been developed for the design and prediction of fusion devices, including SOLPS [1–3], SONIC [4, 5], EDGE2D [6], UEDGE [7], and EMC3-Eirene [8]. Although these codes have been very successful, the simulation of the JT-60U experiment using the SONIC code has overestimated the ion flux at the strike point by a factor of two or more with respect to the experimental value [9]. Some other important quantities have also not been reproduced correctly, from a quantitative point of view. In particular, the radial transport mechanism in the edge plasma has remained unclear, and the experimentally observed diffusion coefficient is about one order of magnitude larger than the theoretically predicted value; hence, this is treated as an anomalous diffusion in the above codes. The radial transport can affect some important quantities, thus influencing the final prediction results. Some models (e.g., [10]) have been proposed to describe the anomalous transport in the SOL.

On the other hand, in edge plasma, neutral particles are generated by recombination, neutralization on the wall, and gas puffing. A neutral particle flux of amplitude equal to or higher than the ion flux has been observed in JT-60U [11]. Elastic scattering between ions and neutral particles can be a large-angle scattering process, and the scat-

tered particle flight direction can be changed significantly in a single scattering event compared with the Coulomb scattering. Figure 1 shows the elastic differential scattering cross sections between deuteron and deuterium [12].

In this work, the probability distribution function [13, 14] (described in section 2.4) was applied to fluid equations for the plasma, and the transport driven by large-angle elastic scattering between ions and neutral particles was studied including the radial direction. Furthermore,

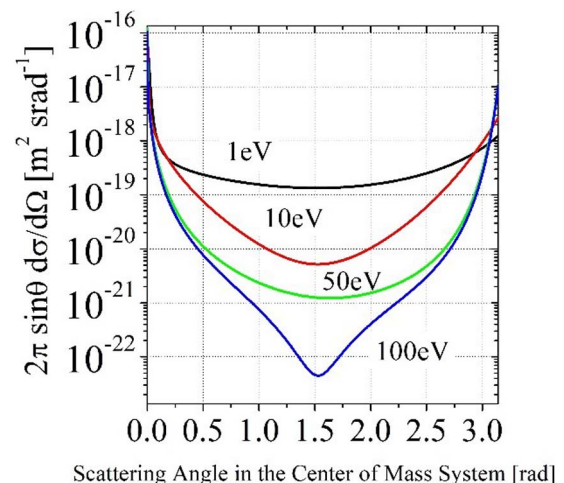


Fig. 1 Elastic differential scattering cross section between deuteron and deuterium [12].

author's e-mail: d_umezaki@nucl.kyushu-u.ac.jp

^{*)} This article is based on the presentation at the 29th International Toki Conference on Plasma and Fusion Research (ITC29).

the influence on the density profile and ion flux at the divertor plate was investigated.

2. Analysis Model

2.1 Calculation scheme and flow

A two-dimensional square scheme ($25 \times 25 \text{ cm}^2$) was implemented to model the divertor plasma region of JT-60U (Fig. 2). The number of numerical cells was set to 10000. Boundary conditions (described in section 2.2) were adopted except for the upstream, and the upstream boundary condition was provided based on the experimental value [9].

The calculation flow consists of the following four steps, as also shown in Fig. 3.

- (0) Initial values of n_i , \vec{u}_i , T_i , and T_e are input. The constant values, such as the diffusion coefficient D , are also input.
- (1) The neutral particles density n_n and temperature T_n are calculated by relating to the plasma density n_i and ion temperature T_i (described in section 2.4). The coefficients determined from the plasma variables, such as the thermal conductivity coefficient, are calculated for the fluid equations.
- (2) The source terms of the fluid equations are computed. In the case of the EL model, S_{EL} , \vec{S}_{PEL} , and S_{iEL} are computed.
- (3) The fluid equations are solved, thus permitting to obtain n_i , \vec{u}_i , T_i , and T_e . In the case of the diffusion model, the radial velocity u_y is computed through the diffusion equation.
- (4) The possible calculation convergence is evaluated. The residual sums of squares (RSS) of n_i , T_i , and T_e between the current and previous steps are computed in all the control volumes. The calculation is considered to be finished when the RSS average in all control volumes is smaller than 10^{-15} , otherwise the calculation flow is repeated starting from step (1).

2.2 Fluid equations

2D fluid equations were used for the plasma. These equations are identical to those in the original B2-code [15], and are based on Braginskii equations [16]. The fluid equations can be written as:

$$\frac{\partial \rho_i}{\partial t} + \nabla \cdot (\rho_i \vec{u}) = S_{\rho_i}, \quad (1)$$

$$\frac{\partial}{\partial t} (\rho_i \vec{u}) + \nabla \cdot (\rho_i \vec{u} \vec{u}) = -\nabla (P_i + P_e) - \nabla \cdot \vec{H} + \vec{S}_p, \quad (2)$$

$$\begin{aligned} & \frac{\partial}{\partial t} \left(\frac{3}{2} n_i T_i + \frac{1}{2} n_i m u^2 \right) + \nabla \cdot \left[\vec{q} + \left(\frac{5}{2} n_i T_i + \frac{1}{2} n_i m u^2 \right) \vec{u} + \vec{H} \cdot \vec{u} \right] \\ & = \vec{u} \cdot \nabla P_e - n_e v (T_i - T_e) + S_i, \end{aligned} \quad (3)$$

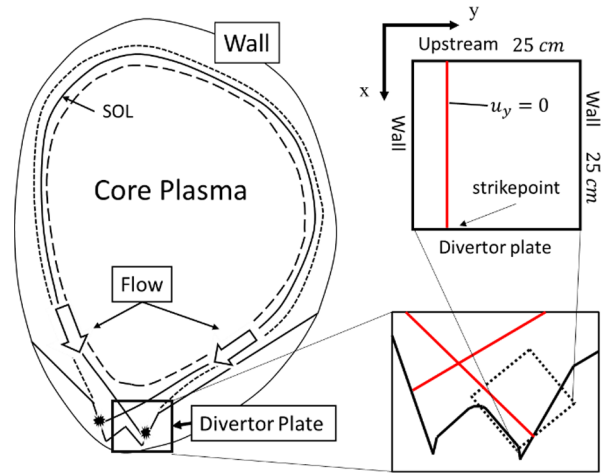


Fig. 2 Calculation scheme with reference to the divertor plasma region of JT-60U.

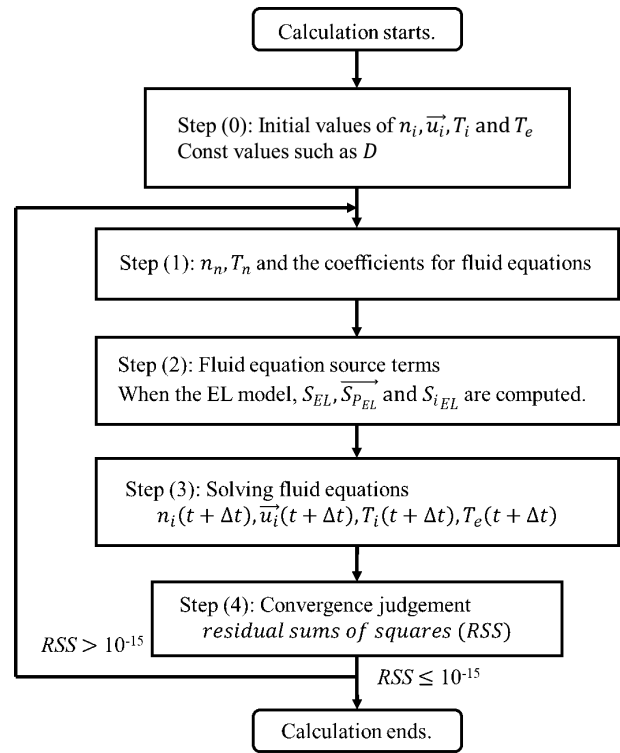


Fig. 3 Calculation flow.

$$\begin{aligned} & \frac{\partial}{\partial t} \left(\frac{3}{2} n_e T_e \right) + \nabla \cdot \left[\frac{5}{2} n_e T_e \vec{u} - k_e \nabla T_e \right] \\ & = \vec{u} \cdot \nabla P_e - n_e v (T_e - T_i) + S_e. \end{aligned} \quad (4)$$

Here, $\vec{u} = (u_x, u_y)$ is the velocity, $n(\rho)$ is the (mass) density, T_i , T_e , P_i , and P_e are the ion and electron temperature, and the ion and electron pressure, respectively. S_{ρ_i} , \vec{S}_p , S_i , and S_e are the source terms, which are written according to:

$$\begin{aligned} S_{\rho_i} &= n_i n_e \langle \sigma v \rangle_{ION} - n_e n_e \langle \sigma v \rangle_{RC} + S_{EL}, \\ \vec{S}_p &= m_i n_n n_i (\langle \sigma v \rangle_{CX} + \langle \sigma v \rangle_{ION}) \cdot \vec{u}_n \end{aligned} \quad (5)$$

$$-m_i n_e n_e (\langle \sigma v \rangle_{RC} + \langle \sigma v \rangle_{CX}) \cdot \vec{u}_i + \vec{S}_{PEL}, \quad (6)$$

$$S_i = n_e n_i (\langle \sigma v \rangle_{ION} + \langle \sigma v \rangle_{CX}) \cdot E_n - n_n n_i (\langle \sigma v \rangle_{RC} + \langle \sigma v \rangle_{CX}) \cdot T_i + S_{iEL}, \quad (7)$$

$$S_e = -n_n n_e \langle \sigma v \rangle_{ION} \cdot \delta_e - n_e n_i \langle \sigma v \rangle_{RC} \cdot T_i. \quad (8)$$

$\langle \sigma v \rangle$ is the reaction rate coefficient. The effects of the elastic scattering S_{EL} , \vec{S}_{PEL} , S_{iEL} are ignored in the diffusion model (described in section 2.3). The subscripts ION, RC, CX, and EL stand for ionization, recombination, charge exchange, and elastic scattering, respectively. $\vec{H} = -\eta_x \nabla_x u_x - \eta_y \nabla_y u_y$ is the viscosity term, $n_e v (T_i - T_e)$ is the equi-partition term, and $\delta_e = 25$ eV.

The boundary conditions at the walls on both sides are as follows:

$$u_x|_{wall} = 0, \quad (9)$$

$$u_y|_{wall} = a_{u_y} \sqrt{\frac{T_i + T_e}{m_i}}, \quad (10)$$

$$\nabla_y n = \frac{n}{\lambda_n}, \quad (11)$$

$$\nabla_y T_{i/e} = \frac{T_{i/e}}{\lambda_{T_{i/e}}}, \quad (12)$$

where λ is the decay length of the ions and electrons. λ_n and $\lambda_{T_{i/e}}$ were both set to 1 cm. α_{u_y} is a freely-selected parameter and was here set to 10^{-3} . The boundary conditions at the divertor plate are as follows [17]:

$$u_x|_{divertor} = \sqrt{\frac{T_i + T_e}{m_i}}, \quad (13)$$

$$\nabla_x n = 0, \quad (14)$$

$$-k_{ix} \nabla_x T_i = \frac{3}{2} n T_i u_x, \quad (15)$$

$$-k_{ex} \nabla_x T_e = 4 n T_e u_x. \quad (16)$$

Here, $k_{ix} = 3.9 n_i T_i \tau_i / m_i$ and $k_{ex} = 3.16 n_e T_e \tau_e / m_e$ are the ions and electrons parallel thermal conductivity coefficients, respectively. τ_i and τ_e are the ion and electron collision time, respectively.

2.3 Diffusion model

In this work, two models were computed for comparison. One model has also been used in the integrated SONIC code to obtain the radial velocity from the diffusion equation. This model is here denoted as the diffusion model. The diffusion equation is written as $u_y = -D/n_i \cdot \nabla n_i$, where $D = 0.3 \text{ m}^2 \text{ s}^{-1}$ is the diffusion coefficient.

In the second model, ions are scattered by neutral particles and fly to other control volumes in various directions, including radial directions, to become a source. This model is here denoted as the EL model (described in section 2.4).

2.4 Large-angle elastic scattering transport model: the EL model

In this model, the ions are treated as a beam having velocity \vec{v}_i' equal to \vec{u}_x and are scattered by neutral parti-

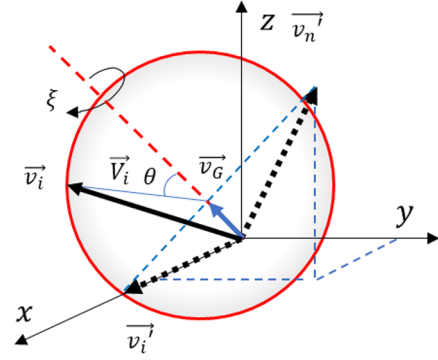


Fig. 4 Schematic view of the change in ion velocity before and after elastic scattering.

cles that have isotropic Maxwellian distribution. Figure 4 shows the change of the ion and neutral particle velocities before and after the elastic scattering. The scattered ion velocity is expressed by the probability distribution function $P(\vec{v}_i' \rightarrow \vec{v}_i | v_n')$ [13, 14]. P represents the probability that an ion velocity changes from \vec{v}_i' to \vec{v}_i as a result of a collision with a neutral particle that has velocity \vec{v}_n' in the laboratory system. In the velocity space, the scattered ion velocity \vec{v}_i lies always on the surface of the sphere that has radius $|\vec{v}_n'|$, with the center of the sphere being located at the end of the center-of-mass velocity \vec{v}_G . The neutral particle velocity \vec{v}_n' is provided using random numbers. The value of the differential cross section $\theta d\sigma/d\Omega(\theta)$ is input into the velocity space cell on the sphere as $P(\vec{v}_i' \rightarrow \vec{v}_i | v_n')$, and P is then normalized so that its integrated value becomes one. The scattered particle velocity distribution per unit time $Q(\vec{v}_i)$ is written as:

$$Q(\vec{v}_i) = \iint \sigma_{EL}(v_r) v_r P(\vec{v}_i' \rightarrow \vec{v}_i | v_n') \times f_i(v_i') f_n(v_n') dv_i' dv_n'. \quad (17)$$

Here, v_r is the relative velocity between \vec{v}_i' and \vec{v}_n' . $Q(\vec{v}_i)$ is determined using P and it is weighed with the neutral particle velocity distribution function $f_n(\vec{v}_n')$, which is assumed to have an isotropic Maxwellian distribution. $f_i(\vec{v}_i') = n_i \delta(\vec{u}_x - \vec{v}_i')$ is the velocity distribution function of the ions. Monte Carlo integration was used for $Q(\vec{v}_i)$. Figure 5 shows $Q(\vec{v}_i)$ integrated over the z direction for the case in which both the ion energy and neutral particle temperature T_n are 10 eV. The ions fly from one control volume to another control volume. $Q(\vec{v}_i)$ has the same dimensions as the Boltzmann collision operator; thus, its integral in the velocity space becomes a source term for a control volume at position $\vec{v}_i \times dt$, as shown in Fig. 6. The density flowing out from the control volume is subtracted. The sum becomes the source term for each control volume. For example, the source terms for the control volume J are written as follows:

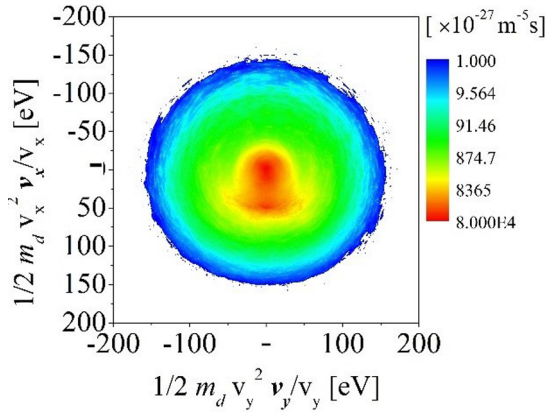


Fig. 5 Example of $\theta(\vec{v}_i)$ integrated over the z direction when the 10 eV ions are scattered by neutral particles with 10 eV Maxwellian distribution.

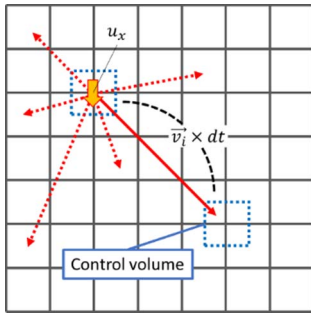


Fig. 6 The ions scattered by neutral particles fly from one control volume to another control volume.

$$S_{PEL}^J = \sum_{k_1=1(k_1 \neq J)}^{mesh} \int_{V_{k_1 \rightarrow J}} Q_{k_1}(\vec{v}_i) d\vec{v}_i - \sum_{k_1=1(k_2 \neq J)}^{mesh} \int_{V_{J \rightarrow k_2}} Q_J(\vec{v}_i) d\vec{v}_i, \quad (18)$$

$$\vec{S}_{PEL}^J = \sum_{k_1=1(k_1 \neq J)}^{mesh} \int_{V_{k_1 \rightarrow J}} m_i \vec{v}_i Q_{k_1}(\vec{v}_i) d\vec{v}_i - n_i n_0 \langle \sigma v \rangle_{EL} \cdot \vec{u}, \quad (19)$$

$$S_{iEL}^J = \sum_{k_1=1(k_1 \neq J)}^{mesh} \int_{V_{k_1 \rightarrow J}} \frac{1}{2} m_i v_i^2 Q_{k_1}(\vec{v}_i) d\vec{v}_i - n_i n_0 \langle \sigma v \rangle_{EL} \frac{1}{2} m v_i^2. \quad (20)$$

2.5 Parameters of the neutral particles

The neutral particles density and temperature are assumed to be $n_n = \alpha_n \times n_i$ and $T_n = \alpha_T \times T_i$, respectively, based on the corresponding parameters α_n and α_T . In this study, $\alpha_n \sim 0.2 - 0.4$ and $\alpha_T \sim 0.1 - 0.5$ were used.

3. Results and Discussion

3.1 Effect on the 2-D profile

The plasma and neutral particles were considered to be only deuteron, electron, and deuterium. Appropriate

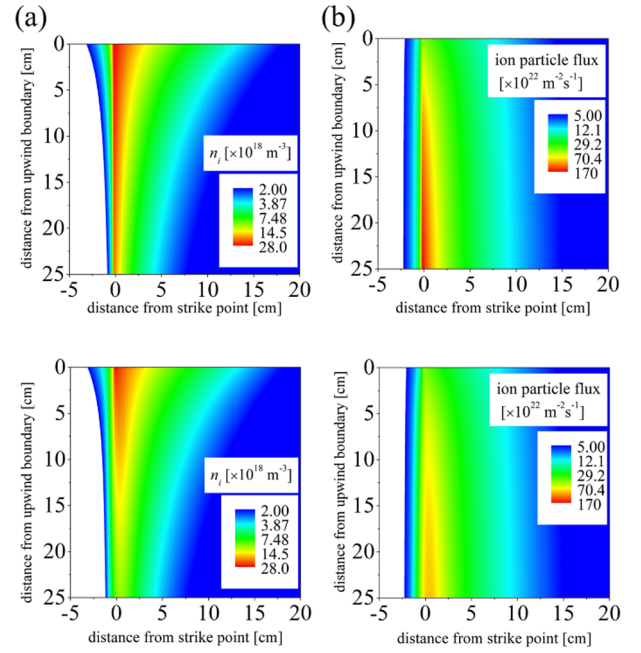


Fig. 7 2-D profile of the (a) plasma density and (b) ion particle flux obtained from the diffusion and EL models.

values for the parameters α_n and α_T were first searched to reproduce the electron density at the divertor plate by the SONIC code. The values were found to be $\alpha_n = 0.4$ and $\alpha_T = 0.3$. The EL model was also simulated with the same parameters. Figures 7 (a) and 7 (b) show the results of the plasma density 2-D profile and ion particle flux obtained from the diffusion model and the EL model, respectively. Each value computed with the EL model is spread in the radial direction, while this is not the case for the diffusion model. In contrast, 2-D profiles of velocity and temperature were not changed significantly. This could be due to the fact that the elastic scattering transport source term is smaller than the other source terms.

3.2 Effect on the ion density profile at the divertor plate

The influence of parameters α_n and α_T on the density profile at the divertor plate was evaluated. Figure 8 shows the profile of the plasma density at the divertor plate obtained with the diffusion and EL models when $\alpha_n \sim 0.2 - 0.4$. In either case, the plasma density near the strike point of the EL model is smaller than that of the diffusion model. Moreover, the density peak is shifted outwards, reflecting a trend that has also been observed in the experiments. As the neutral density becomes larger, the density peak increases, because more ionization events occur.

Figure 9 shows the plasma density profile at the divertor plate obtained with the diffusion and EL models when $\alpha_T \sim 0.1 - 0.5$. In the case of the diffusion model, the change in α_T does not significantly affect the profile. When α_T is large, the density is spread in the radial direction in the EL model, because ions are scattered more strongly in

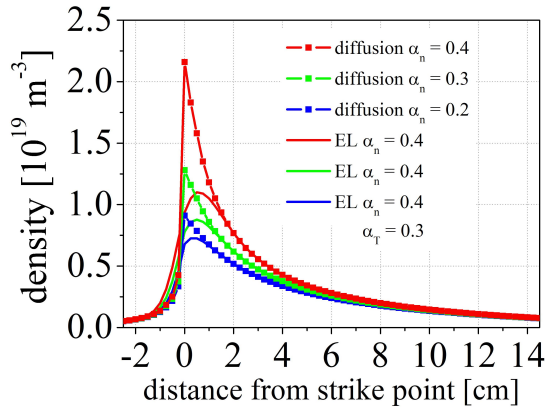


Fig. 8 Comparison of the radial transport effect with different α_n values on the ion density profile at the divertor plate.

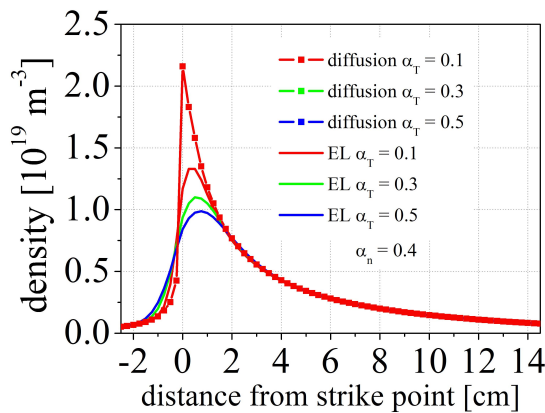


Fig. 9 Comparison of the radial transport effect with different α_T values on the ion density profile at the divertor plate.

the high neutral particle temperature space.

On the other hand, there is almost no effect on the electron temperature when using the EL model. The electron temperature has also been observed to spread in the radial direction in the experiments. In this work, no additional term was used for the electron temperature conservation equation. It will be required for the prediction of quantitative electron temperature to improve the present model.

3.3 Effect on the ion flux peak at the divertor plate

Figure 10 shows the ratio of the ion flux peak at the divertor plate obtained with the diffusion and EL models when $\alpha_T \sim 0.1 - 0.5$. As the temperature of the neutral particles increases, the ratio of the ion flux decreases. This is due to the fact that, when the neutral particle temperature is high, the ions are scattered strongly. The ion flux peak can be reduced to half of the value predicted by the diffusion model by taking the large-angle elastic scattering transport into consideration. The ratio value corresponds to the ratio between the results of the SONIC code and the experimental value.

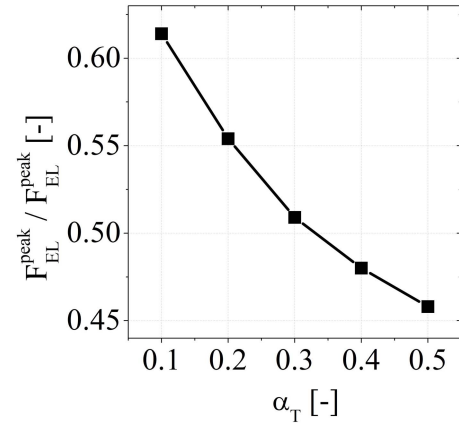


Fig. 10 Relative comparison of the radial transport effect with different α_T values on the ion flux peak at the divertor plate.

4. Conclusions

A transport model driven by the large-angle elastic scattering between ions and neutral particles was proposed. This model may be able to describe the disagreement between simulations and experiments. The 2-D profile of the plasma density and ion flux were found to be spread more extensively in the radial direction using the EL model rather than by the diffusion model. The plasma density peak was reduced to about half of that of the diffusion model.

In contrast, almost no effect was observed on the ion and electron temperature. The electron temperature was also found to spread in the radial direction in the experiments. In this study, no new term was introduced in the source term of the electron energy conservation equation. Further model improvements, including a new term for the electron equation, are needed. In addition, the model needs to be validated by applying the integrated codes.

- [1] A.S. Kukushkin *et al.*, Fusion Eng. Des. **86**, 2865 (2011).
- [2] S. Wiesen *et al.*, J. Nucl. Mater. **463**, 480 (2015).
- [3] X. Bonnin *et al.*, Plasma Fusion Res. **11**, 1403102 (2016).
- [4] H. Kawashima *et al.*, Plasma Fusion Res. **1**, 031 (2006).
- [5] K. Shimizu *et al.*, Nucl. Fusion **49**, 3403070 (2009).
- [6] A. Taroni *et al.*, Contrib. Plasma Phys. **32**, 438 (1992).
- [7] T.D. Rognlien *et al.*, Contrib. Plasma Phys. **34**, 362 (1994).
- [8] Y. Feng *et al.*, J. Nucl. Mater. **266**, 812 (1999).
- [9] K. Hoshino *et al.*, J. Nucl. Mater. **463**, 573 (2015).
- [10] S. Baschetti *et al.*, Nucl. Mater. Energy **19**, 200 (2019).
- [11] T. Takizuka *et al.*, JAERI-Research 2003-010.
- [12] P.S. Kristić and D.R. Schultz, At. Plasma-Mat. Interact. Data Fusion **8**, 1 (1992).
- [13] H. Matsuura and Y. Nakao, Phys. Plasmas **13**, 062507 (2006).
- [14] H. Matsuura *et al.*, Plasma Fusion Res. **11**, 1403105 (2016).
- [15] B.J. Braams, NET Rep. 68 EURFU/XII-80/87/68, CEC, Brussels (1987).
- [16] S.I. Braginskii, Trans. Processes Plasma Rev. of Plasma Phys. **1**, 205 (1965).
- [17] R. Schnelder *et al.*, Contrib. Plasma Phys. **46** 1 (2006).